

First-return statistics in Henyey–Greenstein scattering: Motzkin polynomials and the Cauchy kernel

C Zeller¹ and R Cordery²

¹ Claude Zeller Consulting LLC, Tillamook, Oregon 97134, USA

² Department of Physics, Fairfield University, Fairfield, Connecticut 06824, USA

E-mail: czeller@ieee.org, rcordery@fairfield.edu

Abstract

In our previous work [Zeller and Cordery 2020 *J. Stat. Mech.* **2020** 063404], we established that first-return probabilities in 1D scattering expand in Catalan and Motzkin numbers. Extending this framework to 3D Henyey–Greenstein scattering requires a Boundary Truncation Factor (BTF): boundary constraints reduce the effective anisotropy from g^n to $g^n \cdot \text{BTF}(n, g)$. Monte Carlo simulations (10^{12} scattering events) reveal that the BTF follows a Cauchy kernel with width $m_x(g) = 4g/(1-g)$, amplitude $A(g) = 1 - g(1+g)/2$, and peak at scattering order $n = 2$. This form achieves 1–2% accuracy for $g < 2/3$; five parameters capture the entire parameter space ($2 \leq n \leq 100$, $0 \leq g \leq 0.95$). A first-principles derivation remains open. The closed-form BTF replaces Monte Carlo in iterative inverse problems, enabling orders-of-magnitude speed-up.

Keywords: first-passage problem, random walk, Cauchy kernel, Motzkin polynomials, radiative transfer, Henyey–Greenstein scattering

1 Introduction

First-passage problems appear throughout statistical mechanics—in polymer physics, diffusion-limited aggregation, financial mathematics, and queueing theory [1, 2, 3]. A clean example arises in radiative transport: photons entering a scattering medium execute a three-dimensional random walk and may return to the entry boundary. The statistics of this first-passage event encode how stochastic motion interacts with geometric constraint.

Throughout, “first-return” means first passage back to $z = 0$ from $z > 0$ with negative z -velocity—the photon must exit, not graze inward.

In our previous work in this journal [6], we established that first-return probabilities in one-dimensional isotropic scattering expand in Catalan numbers, the combinatorial objects counting Dyck paths. The reflectance of a semi-infinite Kubelka–Munk medium [7] admits the generating function representation

$$R_\infty(S, \chi) = \frac{1}{2} \cdot \frac{S}{S + \chi} \cdot C\left(\frac{S^2}{4(S + \chi)^2}\right) \quad (1.1)$$

where $C(x) = \sum_{n=0}^{\infty} C_n x^n$ is the Catalan generating function [17] and $C_n = (2n)!/(n!(n+1)!)$. This is distribution-free: it depends only on the zigzag structure, not step lengths.

Forward-peaked scattering introduces “flat” steps—events preserving the sign of z -velocity. The Motzkin extension [14, 15] handles this, giving

$$P_{\text{refl}}^{(1D)}(n, r) = M_{n-2} \left(\frac{1-2r}{r} \right) \cdot \left(\frac{r}{2} \right)^{n-1} \quad (1.2)$$

where $M_n(t)$ is the Motzkin polynomial and r the backward-step probability.

The central challenge is extending this framework to *three-dimensional anisotropic* scattering governed by the Henyey–Greenstein phase function [12]. Direct embedding of Motzkin structure via an effective backscattering coefficient $r_b(g)$ fails; as we show below, the mapping requires a **Boundary Truncation Factor** (BTF) that accounts for geometric constraints at the boundary.

We show that the BTF follows a **Cauchy kernel** in the scattering order n :

$$\text{BTF}(n, g) = \frac{A(g)}{1 + \left(\frac{n-n_0}{m_x(g)} \right)^2} \quad (1.3)$$

with parameters expressible in terms of the anisotropy factor g alone:

$$m_x(g) = \frac{4g}{1-g} \quad (\text{width}) \quad (1.4)$$

$$A(g) = 1 - \frac{g(1+g)}{2} \quad (\text{amplitude}) \quad (1.5)$$

$$n_0 = 2 \quad (\text{peak location}) \quad (1.6)$$

The simple integer coefficients suggest underlying geometric structure; however, a first-principles derivation of the Cauchy form remains an open problem (Section 7.1).

The theory applies for $g \lesssim 2/3$ and $n \geq 2$; above $g \approx 2/3$, deviations grow gradually but can be corrected by a modified Cauchy kernel with a shape parameter (Section 6).

Practical scope of the validity range. The constraint $g < 2/3$ complements rather than competes with biological tissue optics, where $g \approx 0.9$ –0.98 is typical [21]. Table 1 summarizes representative anisotropy factors for various scattering media. Many industrial and environmental applications fall within the validity range of the present theory; for higher-anisotropy materials, the Cauchy kernel form remains valid but parameters benefit from Monte Carlo calibration (Section 4).

Table 1: Representative anisotropy factors g for various scattering media.

Material	g	Reference
<i>Within validity range ($g < 2/3$)</i>		
Isotropic scatterers	0	Definition
Paper / print media	0.4–0.6	[22]
<i>Above validity range ($g > 2/3$)</i>		
Human dermis/epidermis	0.7–0.9	[20]
Biological tissue (in vivo)	0.9–0.98	[21]
Intralipid phantoms	~ 0.9	Standard value

Table 2: Progression of results from [6] through the present work.

Aspect	Zeller & Cordery (2020)	Present work
Dimension	1D	$3D \rightarrow 1D$ via BTF
Scattering	Isotropic + forward bias	Henyey–Greenstein
Combinatorics	Catalan \rightarrow Motzkin	Motzkin + BTF correction
BTF	Not needed	Cauchy kernel (empirical)
Incidence	Normal only	Normal only
Validity range	—	$g < 2/3$ (Cauchy); $g < 0.95$ (modified)
Status	Derived	Empirical; derivation open

1.1 Relation to previous work

Table 2 summarizes the progression from [6].

From our 2020 paper, we carry forward: (i) the Motzkin polynomial framework (equation (1.2)); (ii) the distribution-free character of first-passage combinatorics; and (iii) the connection to classical fluctuation theory [5, 4]. What is new here is: (i) identification of the Cauchy kernel form for the BTF through systematic model selection; (ii) determination of the parameters $m_x(g)$ and $A(g)$ from Monte Carlo fitting; and (iii) a modified Cauchy kernel extending validity to high anisotropy.

1.2 Comparison with generalized Kubelka–Munk

Our approach differs from previous 3D extensions of Kubelka–Munk. Sandoval and Kim [9, 10] extended KM through double spherical harmonics (DP_1), obtaining an 8×8 system for forward and backward power flow. For isotropic scattering in optically thick media, their generalized KM achieves errors below 15% when $z_0 \geq 10$ (where z_0 is the optical thickness).

However, DP_1 encounters difficulties for anisotropic scattering. Its basis functions contain only first-order azimuthal harmonics and cannot capture forward-peaked phase functions. At $g = 0.8$, Sandoval and Kim found errors exceeding 80% in transmitted power; at higher anisotropy, the approximation gives negative intensities.

The BTF framework inverts the dimensional strategy: instead of enriching 1D equations with 3D coupling, we use 1D combinatorics and correct for boundary truncation. Table 3 compares the two approaches.

Table 3: Comparison of dimensional reduction strategies for semi-infinite media.

Property	gKM (Sandoval & Kim)	BTF (this work)
Geometry	Finite slab	Semi-infinite
Strategy	$1D \rightarrow 3D$ extension	$3D \rightarrow 1D$ reduction
Angular basis	DP_1 (4 func./hemisphere)	HG sampling + Motzkin
Isotropic limit	<15% error for $z_0 \geq 10$	Recovers Catalan structure
Anisotropic range	$g \lesssim 0.5$ (qualitative)	$g < 2/3$ (<2% deviation)
High- g behavior	Unphysical (negative values)	Predictable drift
Incidence	Oblique via eigenmode	Normal (oblique: future work)
Computational form	8×8 PDE system	1D polynomial evaluation

Practitioner guidance. For semi-infinite media with $g \lesssim 2/3$, BTF+Motzkin is more accurate than DP_1 : 1D polynomial evaluation achieves sub-2% accuracy versus 15%+ for gKM. For finite slabs or strong absorption, use gKM or Monte Carlo. BTF excels in inverse problems requiring thousands of transport evaluations.

1.3 Paper organization

Section 2 reviews the 1D Motzkin framework [6]. Section 3 introduces the Boundary Truncation Factor and its Cauchy kernel form. Section 4 describes the Monte Carlo procedure. Section 5 presents the computational algorithm. Section 6 presents the modified Cauchy kernel for high-anisotropy scattering ($g > 2/3$). Section 7 concludes.

2 One-dimensional theory: Catalan and Motzkin structures

We review results from [6]; see [1, 2] for background.

2.1 Kubelka–Munk reflectance and Catalan numbers

The Kubelka–Munk equations [7, 11] describe one-dimensional radiative transport with isotropic scattering:

$$\begin{pmatrix} dI \\ dJ \end{pmatrix} = \begin{pmatrix} -(S + \chi) & S \\ -S & (S + \chi) \end{pmatrix} \begin{pmatrix} I \\ J \end{pmatrix} dz \quad (2.1)$$

where I and J are forward and backward fluxes, S the scattering coefficient, and χ the absorption coefficient. The reflectance of a semi-infinite slab is

$$R_\infty(S, \chi) = \frac{S + \chi}{S} - \sqrt{\left(\frac{S + \chi}{S}\right)^2 - 1} \quad (2.2)$$

The key result of [6] is that this reflectance expands in Catalan numbers:

$$R_\infty(S, \chi) = \sum_{n_p=1}^{\infty} \frac{C_{n_p-1}}{2^{2n_p-1}} \left(\frac{S}{S + \chi}\right)^{2n_p-1} \quad (2.3)$$

Photon trajectories form zigzag random walks; first passage occurs at the first backward crossing of $z = 0$. The probability at the n_p -th peak is $P(n_p) = C_{n_p-1}/2^{2n_p-1}$, connecting to Spitzer’s identity [3] and Andersen’s equivalence principle [5].

2.2 Motzkin extension for forward scattering

Catalan numbers count Dyck paths—walks restricted to up- and down-steps. Forward scattering introduces flat steps (events preserving the sign of z -velocity), requiring the Motzkin extension [14, 15, 16].

Definition (Motzkin polynomial). The Motzkin polynomial of degree n is

$$M_n(t) = \sum_{k=0}^{\lfloor n/2 \rfloor} T(n, k) \cdot t^{n-2k} \quad (2.4)$$

where $T(n, k)$ are the Motzkin triangle coefficients [17]:

$$T(n, k) = \frac{n!}{(n-2k)! k! (k+1)!} \quad (2.5)$$

The one-dimensional first-return probability with forward scattering becomes equation (1.2), encoding three processes: up-steps (positive z -projection), down-steps (negative z -projection), and flat steps (zero z -projection change).

3 The Boundary Truncation Factor

The Motzkin framework applies to one-dimensional scattering. To use it for three-dimensional Henyey–Greenstein transport, we need a mapping—an effective backscattering coefficient $r_b(g, n)$ that makes the 1D formula reproduce 3D first-return probabilities. This section introduces the Boundary Truncation Factor (BTF), the correction that makes this mapping work.

3.1 Physical origin

In bulk scattering without boundaries, Pfeiffer and Chapman [13] proved that the Henyey–Greenstein phase function is closed under successive scattering: after n scattering events, the angular distribution of the scattering cosine $\cos \theta = \boldsymbol{\Omega}_0 \cdot \boldsymbol{\Omega}_n$ is itself a Henyey–Greenstein distribution with parameter g^n :

$$p_n(\cos \theta; g) = P_{\text{HG}}(\cos \theta; g^n) \quad (3.1)$$

This closure property—not merely the statement $\langle \cos \theta \rangle = g^n$ —underlies the dimensional reduction from 3D to 1D.

First-passage problems impose geometric constraints that modify this relationship. The requirement that photons return to their entry boundary restricts the accessible angular phase space: trajectories that wander too far forward are less likely to return. This geometric truncation breaks the closure property, effectively reducing the asymmetry parameter beyond the bulk value:

$$g_{\text{eff}}^{(\text{constrained})} = g^n \cdot \text{BTF}(n, g) \quad (3.2)$$

where $\text{BTF} \leq 1$ represents the multiplicative reduction due to boundary constraints. In the bulk limit (no boundary), $\text{BTF} = 1$ and we recover equation (3.1); at a boundary, the incomplete angular integration yields $\text{BTF} < 1$.

Formally, the BTF emerges from boundary-constrained angular integration:

$$\text{BTF}(n, g) = \frac{\int \cdots \int \prod_{i=1}^n P_{\text{HG}}(\mu_i; g) \times [\text{return constraint}] \, d\mu_1 \cdots d\mu_n}{\int \cdots \int \prod_{i=1}^n P_{\text{HG}}(\mu_i; g) \, d\mu_1 \cdots d\mu_n} \quad (3.3)$$

where the constraint ensures the photon crosses below $z = 0$ after exactly n scattering events. These nested integrals become analytically intractable beyond $n = 3$.

3.2 Empirical discovery

Since direct evaluation of equation (3.3) is impractical, we determined BTF empirically. Monte Carlo simulations provide exact first-return probabilities for 3D photon transport. The simulations covered $g \in [0.05, 0.95]$ (19 values) and $n \in [2, 100]$ (99 values) with 10^8 trajectories per g value and 10 independent runs—approximately 10^{10} photon histories (10^{12} scattering events, ~ 500 CPU-hours).

For each (g, n) pair, we extracted the BTF as the value needed to make the 1D Motzkin formula reproduce the Monte Carlo 3D result:

$$P_{3D}^{(MC)}(n, g) = P_{1D}^{(\text{Motzkin})}(n, r_b(g, n)) \quad (3.4)$$

where $r_b(g, n)$ depends on BTF through the effective anisotropy.

3.3 The Cauchy kernel

Systematic model selection—starting with high-order Padé approximants (rational polynomial fits) and progressively reducing complexity while monitoring cross-validation error—revealed that the optimal functional form is a Cauchy kernel:

$$\text{BTF}(n, g) = \frac{A(g)}{1 + \left(\frac{n-2}{m_x(g)}\right)^2} \quad (3.5)$$

with parameters:

$$A(g) = 1 - \frac{g(1+g)}{2} = \frac{(1-g)(2+g)}{2} \quad (\text{amplitude}) \quad (3.6)$$

$$m_x(g) = \frac{4g}{1-g} \quad (\text{width}) \quad (3.7)$$

The peak location $n_0 = 2$ corresponds to the minimum scattering order for first return. This parameterized form reproduces Monte Carlo-derived BTF values with mean deviation $<2\%$ and cross-validated $R^2 > 0.999$ for $g \leq 2/3$.

Statistical evidence for integer coefficients. The 10 independent Monte Carlo runs allow statistical testing of the numerical coefficients. Fitting across all runs yields $n_0 = 2.2 \pm 0.3$ and width prefactor 3.9 ± 0.3 ; the integers 2 and 4 both lie within one standard deviation of the fitted values. (The exponent 2 in the denominator emerged from the Padé approximant model selection, not from parameter fitting.) This suggests exact integer structure rather than numerical coincidence.

Limiting behavior. For short paths ($n - 2 \ll m_x$), $\text{BTF} \approx A(g)$ with minimal boundary effects. For long paths ($n - 2 \gg m_x$), $\text{BTF} \rightarrow 0$ as boundary truncation dominates. At $g = 0$ (isotropic), $A = 1$ and $m_x = 0$, so $\text{BTF} = 1$ for $n = 2$ and $\text{BTF} = 0$ for $n > 2$ —reflecting that isotropic scattering requires exactly two steps for first return.

Figure 1 shows the BTF directly as a function of scattering order n for several anisotropy values. The Cauchy profile is evident: a peak at $n = 2$ with power-law decay at large n .

4 Monte Carlo procedure

This section details the Monte Carlo simulations from which the BTF was extracted.

4.1 Simulation procedure

We follow the standard Monte Carlo procedure for photon transport [18]. First return occurs when z first becomes negative [19]. Photons are initialized at the origin ($z = 0^+$) with direction cosine $\mu_0 = 1$. At each scattering event, path length is sampled from $p(c) = e^{-c}$ (unit mean free path) and scattering angle from the Henyey–Greenstein phase

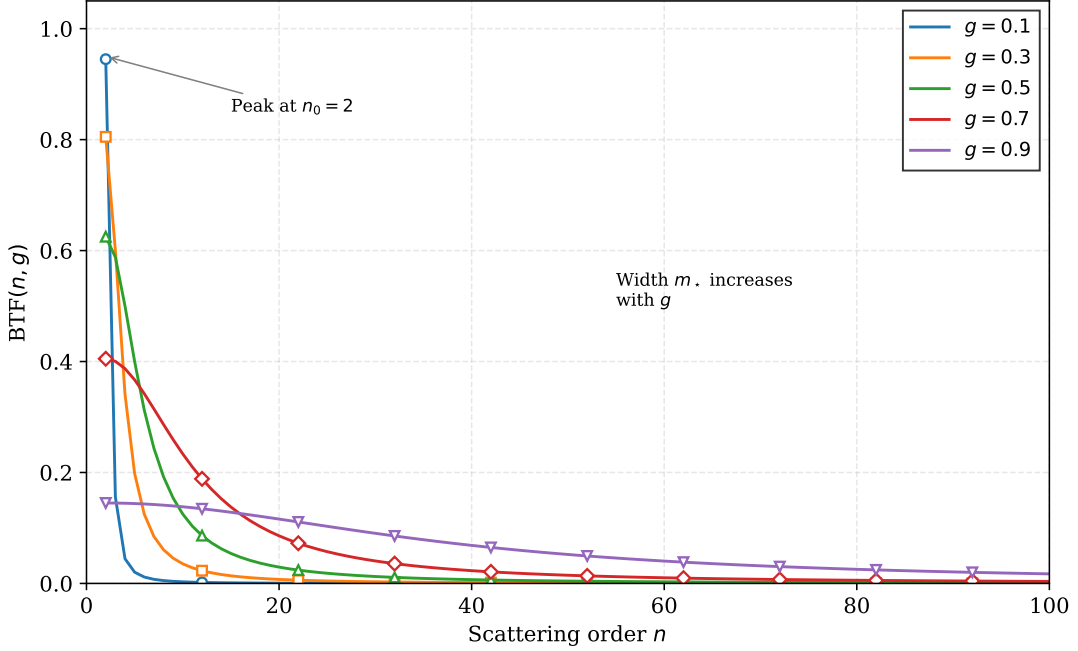


Figure 1: The Boundary Truncation Factor versus scattering order n for $g = 0.1, 0.3, 0.5, 0.7, 0.9$. Points: extracted from Monte Carlo. Curves: Cauchy kernel (equation 3.5). The width $m_x(g)$ increases with g ; the amplitude $A(g)$ decreases. At $g = 0.9$, deviations from Cauchy become visible. (Figures use “path length m_s ” following MC convention; $m_s \equiv n$.)

function via inverse CDF. The scattering order n is recorded at first occurrence of $z < 0$. We simulated 10^8 trajectories per g value with 10 independent runs.

The Henyey–Greenstein phase function is

$$P_{\text{HG}}(\mu; g) = \frac{1 - g^2}{2(1 + g^2 - 2g\mu)^{3/2}}, \quad -1 \leq \mu \leq 1 \quad (4.1)$$

where $g = \langle \mu \rangle \in [0, 1]$ is the anisotropy parameter.

4.2 Fit quality

The Cauchy kernel captures the Monte Carlo data with mean deviation $< 2\%$ for $g < 2/3$. Table 4 shows the root-mean-square error (RMSE) and coefficient of determination (R^2) at representative g values.

Table 4: Fit quality of the Cauchy BTF versus Monte Carlo.

g	RMSE	R^2	Max deviation
0.10	3.2×10^{-4}	0.9998	1.1%
0.30	4.1×10^{-4}	0.9997	1.4%
0.50	4.8×10^{-4}	0.9996	1.8%
$\frac{2}{3}$	5.2×10^{-4}	0.9994	2.1%
0.80	8.3×10^{-4}	0.9985	5.2%
0.90	2.2×10^{-3}	0.9941	14.8%

Error bounds. For $g < 2/3$, root-mean-square deviation is below 2% across all n . For $g > 2/3$, errors grow approximately as $\epsilon(g) \approx 0.05 \cdot (g - 2/3)/(1 - g)$, reaching $\sim 15\%$ at $g = 0.9$. For $g > 0.8$, the modified kernel (Section 6) is recommended.

5 Computational algorithm

We present the complete algorithm for mapping 3D Henyey–Greenstein scattering to 1D Motzkin combinatorics. The algorithm has four steps: (1) determine the angular threshold separating forward from backward scattering; (2) compute the BTF-modified exponent; (3) evaluate the effective backscattering probability; (4) apply the Motzkin formula.

Step 1 (Angular threshold): The threshold $\mu_b(g)$ is the direction cosine separating “effective backward” from “effective forward” scattering in the 1D projection. Physically, μ_b partitions the angular phase space so that the 1D Motzkin counting matches the 3D return statistics. Solve

$$p_{r2}(g) - \frac{1}{2}F(-\mu_b; g^2) = 0 \quad (5.1)$$

where $p_{r2}(g) = \int_{-1}^0 \frac{\mu' - 1}{\mu'} P_{\text{HG}}(\mu', g) d\mu'$ is the exact two-step return probability, $F(\mu; g)$ is the HG cumulative distribution function, and g^2 appears because after two scattering events the angular distribution has parameter g^2 (equation 3.1).

Step 2 (Effective exponent): In bulk scattering, the effective anisotropy after n events is g^n (standard convolution). Near a boundary, transverse filtering reduces this—captured by the BTF. We model the boundary-constrained effective exponent as

$$\gamma(g, n) = 2 + \text{BTF}(n, g)(n - 2) \quad (5.2)$$

This interpolates between $\gamma = 2$ at $n = 2$ (where $\text{BTF} = A(g)$ is maximal and the constraint is weakest) and $\gamma \rightarrow 2$ as $n \rightarrow \infty$ (where $\text{BTF} \rightarrow 0$ and boundary truncation dominates). The baseline $\gamma = 2$ reflects the minimum scattering order for first return. This ansatz is empirically motivated: it produces the correct limits and matches Monte Carlo across the parameter space.

Step 3 (Effective backscattering): Substitute into the HG CDF:

$$r_b(g, n) = F(-\mu_b(g); g^{\gamma(g, n)}) \quad (5.3)$$

Step 4 (First-return probability): The 3D first-return probability follows from equation (1.2) with the effective backscattering:

$$P_{\text{3D}}^{(\text{refl})}(g, n) = M_{n-2} \left(\frac{1 - 2r_b}{r_b} \right) \cdot \left(\frac{r_b}{2} \right)^{n-1} \quad (5.4)$$

This maps 3D Henyey–Greenstein scattering to 1D Motzkin combinatorics.

Isotropic limit check. At $g = 0$: $m_x = 0$, $A = 1$, so $\text{BTF} = 1$ for $n = 2$ and $\text{BTF} = 0$ for $n > 2$. The effective exponent becomes $\gamma = 2$ for all n . The threshold $\mu_b(0) = 0$ (hemisphere boundary), giving $r_b = 1/2$. Substituting into equation (5.4) with $r_b = 1/2$ recovers the Catalan first-return probabilities of [6], confirming internal consistency.

6 High-anisotropy extension: Modified Cauchy kernel

The Cauchy BTF derived in Section 3.3 works to 2% for $g < 2/3$. Biological tissue has $g \approx 0.9\text{--}0.98$ [20, 21], outside this range. Here we develop a one-parameter extension that reduces errors by roughly half at high g .

6.1 Systematic deviations at high g

Data from 10^{12} scattering events show systematic deviations from Cauchy at high g . Figure 2 plots $(P_{\text{MC}} - P_{\text{Cauchy}})/P_{\text{Cauchy}}$ against $(n - 2)/m_x$: for $g > 0.85$, Monte Carlo runs high near the peak and low in the tail—lighter tails than Cauchy.

One possible interpretation: strongly forward-peaked scattering may suppress the long, wandering trajectories that populate the Cauchy tail. Photons that scatter many times at high g tend to propagate forward and are less likely to return (ballistic regime); those that do return must do so in relatively few steps. This remains conjecture; a rigorous derivation is lacking.

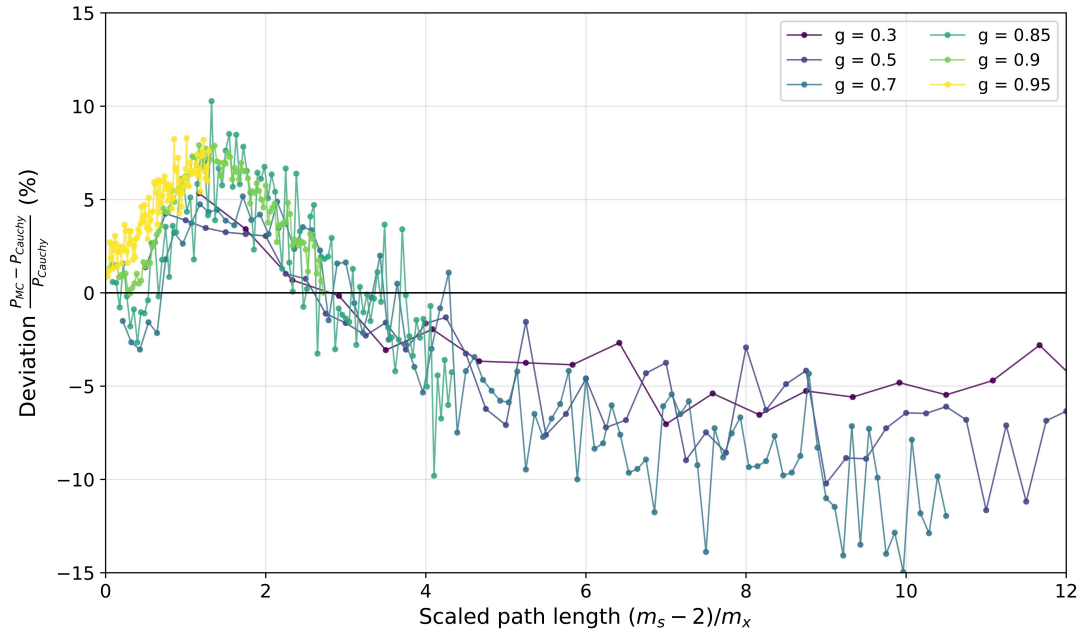


Figure 2: Deviations from the Cauchy kernel versus scaled path length. At high g , Monte Carlo runs high near the peak and low in the tail—the signature of lighter-than-Cauchy tails.

6.2 Modified Cauchy kernel

The generalization lets the exponent vary:

$$K_\alpha(x) = \frac{1}{[1 + x^2]^{(1+\alpha)/2}} \quad (6.1)$$

with shape parameter α . Setting $\alpha = 1$ recovers Cauchy; $\alpha > 1$ gives faster tail decay. This “generalized Cauchy” appears in robust statistics [23, 24]. Note that α is a shape parameter, not a Lévy stability index.

The modified BTF becomes

$$\text{BTF}_\alpha(n, g) = \frac{A(g)}{\left[1 + \left(\frac{n-2}{m_x(g)}\right)^2\right]^{(1+\alpha(g))/2}} \quad (6.2)$$

with $A(g)$ and $m_x(g)$ unchanged.

6.3 Fitting the shape parameter

We fit α at each g by least squares against Monte Carlo. The results follow

$$\alpha(g) = 1 + 0.033 \cdot \frac{g - \frac{2}{3}}{1 - g} \quad (6.3)$$

Table 5 compares fitted and calculated values. The parameter stays close to unity: $\alpha \approx 0.98$ at low g , rising to $\alpha \approx 1.2$ at $g = 0.95$.

Table 5: Fitted α versus formula (6.3).

g	m_x	α (fitted)	α (formula)	$(1 + \alpha)/2$
0.10	0.4	0.981	0.979	0.99
0.30	1.7	0.990	0.983	0.99
0.50	4.0	0.990	0.989	0.99
$\frac{2}{3}$	8.0	—	1.000	1.00
0.80	16	1.018	1.022	1.01
0.90	36	1.090	1.078	1.04
0.95	76	1.196	1.189	1.09

Figure 3 compares Monte Carlo path length distributions with both Cauchy ($\alpha = 1$) and α -corrected fits. At low g , the curves overlap; at high g , the α -corrected fit (dashed) tracks the data while Cauchy (solid) systematically deviates.

The crossover $\alpha = 1$ occurs at $g = 2/3$, where the Cauchy BTF begins to deviate.

The formula contains the factor $1/(1 - g) = \ell^*/\ell$, where ℓ is the scattering mean free path and $\ell^* = \ell/(1 - g)$ is the transport mean free path. This ratio appears throughout radiative transfer theory as the natural length scale for direction randomization [8]. Its emergence in the shape parameter suggests a connection to Chandrasekhar's similarity principle: transport properties depend on g primarily through ℓ^* , not ℓ and g separately. Figure 4 plots α against this variable; $\alpha = 1$ occurs at $\ell^*/\ell = 3$.

We stress that equation (6.3) is an empirical fit, not a derivation. It minimizes squared error across all n and captures the trend; the coefficient 0.033 is a fitted constant without theoretical explanation.

6.4 Practical recommendations

Guidelines for implementation:

- $g < 0.85$: use the standard Cauchy BTF. Errors remain under 2%, and the formula is simpler.
- $0.85 \leq g \leq 0.95$: use the modified form with α from equation (6.3). RMSE improves by $\sim 45\%$.
- $g > 0.95$: the formula has not been validated beyond $g = 0.95$. Monte Carlo calibration is recommended.

For tissue optics ($g \approx 0.9$ –0.95), the modified kernel extends the analytical BTF into the regime of primary interest.

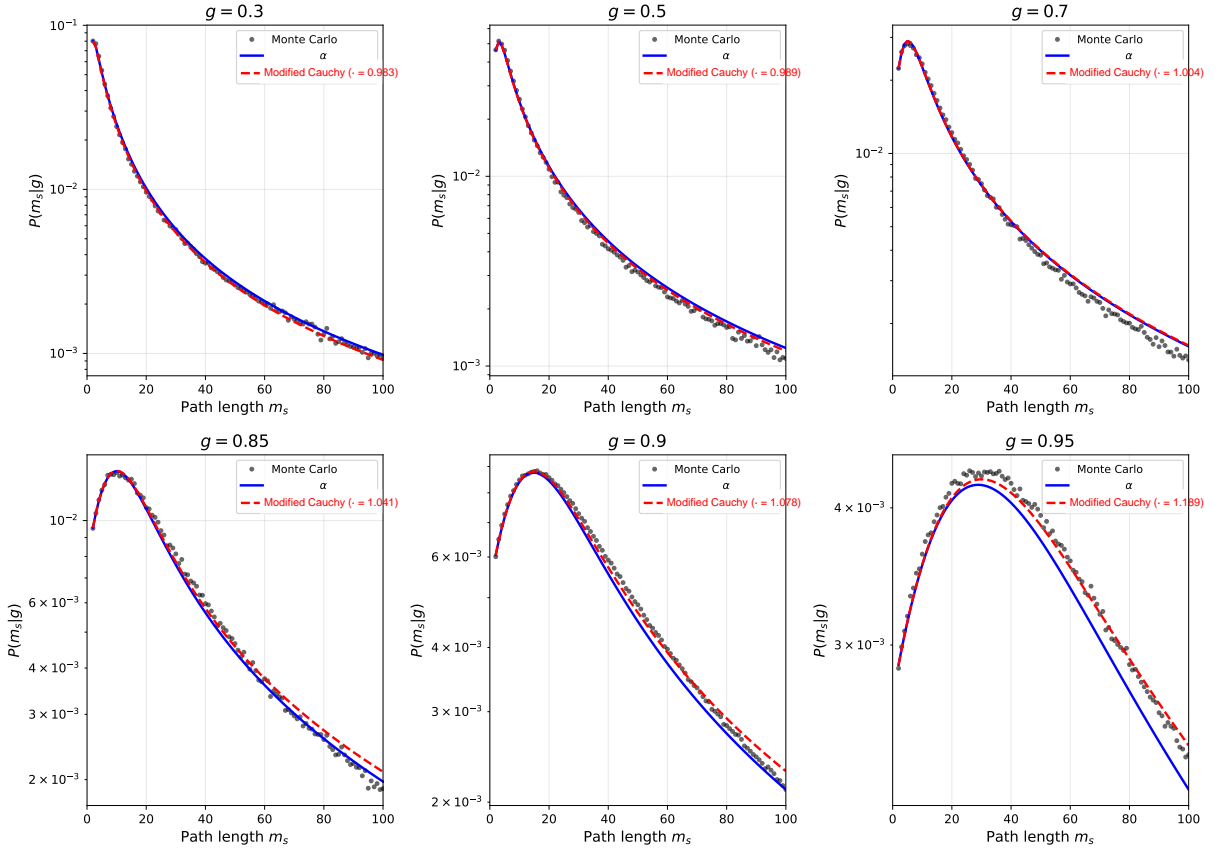


Figure 3: Path length distributions $P(m_s|g)$ for six anisotropy values. Gray points: Monte Carlo. Blue solid: Cauchy kernel ($\alpha = 1$). Red dashed: Modified Cauchy kernel. At $g \leq 0.7$, the curves are indistinguishable; at $g \geq 0.85$, the modified kernel captures the lighter tails.

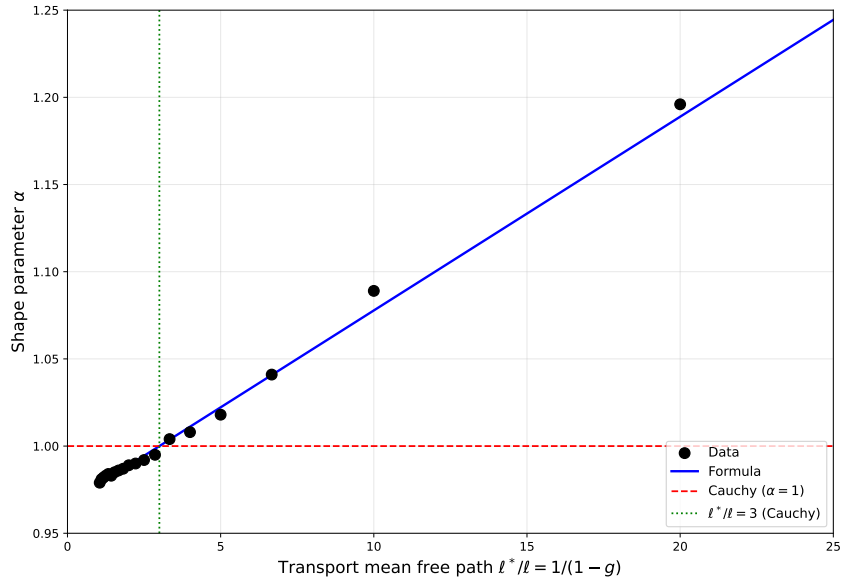


Figure 4: Shape parameter α versus transport mean free path ratio $\ell^*/\ell = 1/(1-g)$. The Cauchy case $\alpha = 1$ occurs at $\ell^*/\ell = 3$.

7 Conclusions

The central empirical result is that the Boundary Truncation Factor for 3D Henyey–Greenstein scattering takes a Cauchy kernel form, with parameters $n_0 = 2$, $m_x = 4g/(1-g)$, and $A(g) = 1 - g(1+g)/2$. Monte Carlo simulations with 10^{12} scattering events confirm this to 1–2% accuracy for $g < 2/3$. The parsimony is remarkable: just five parameters capture the entire parameter space ($n = 2$ –100, $g = 0$ –0.95).

The BTF corrects for transverse diffusion, which reduces return probability at large n . The Cauchy form emerges robustly from Monte Carlo. Why this form, and not another, remains open.

For high anisotropy ($g > 2/3$), a modified Cauchy kernel with shape parameter $\alpha(g)$ extends the theory to $g \approx 0.95$, covering biological tissue. The high- g extension is phenomenological but constrained by Monte Carlo data—not a free fit.

In practice, the framework replaces 3D Monte Carlo with 1D polynomial evaluation, useful for inverse problems requiring many transport calculations [20, 22].

7.1 Open problems

Several points lack theoretical foundation:

(1) Why Cauchy? The Cauchy kernel emerges empirically but is not derived from first principles. The geometric mechanism—transverse filtering—is clear, but why it produces precisely the Cauchy form (rather than Gaussian, exponential, or other) is unexplained.

(2) Amplitude formula. The expression $A(g) = 1 - g(1+g)/2$ comes from fitting. A derivation from hemisphere geometry and flux balance would be more satisfying.

(3) Width formula. The factor 4 in $m_x = 4g/(1-g)$ may decompose as 2×2 : one factor from $\langle c^2 \rangle / \langle c \rangle^2 = 2$ (exponential path lengths), one from first-passage geometry. The geometric factor awaits rigorous analysis.

(4) Shape parameter formula. The empirical fit $\alpha(g) = 1 + 0.033(g - 2/3)/(1-g)$ works but is unexplained. The coefficient 0.033 is a fitted constant without evident geometric meaning, unlike the integer coefficients in the Cauchy kernel.

The integer coefficients (2, 4) in the Cauchy kernel are not rounded values but the closest integers compatible with fitting statistics across 10 independent Monte Carlo runs (Section 3.3). This statistical evidence, combined with the appearance of the Cauchy kernel, suggests that a clean derivation may exist, perhaps through first-passage theory for 3D random walks. We leave this as a challenge for future work.

(5) Oblique incidence. The present work addresses normal incidence only. Extending the Motzkin framework to oblique incidence—where transverse activity n_{xy} couples to the return statistics—requires higher-order Motzkin polynomials, making parameter calculation considerably more challenging. This is an important next step requiring both theoretical development and Monte Carlo validation.

Acknowledgements

CZ thanks Dr. Florence Zeller for discussions on Chebyshev polynomials and Motzkin structures, Professor Arnold Kim for encouragement and guidance, and Professor Michel Talagrand for perspective on the difficulty of proving the Cauchy kernel rigorously.

A Notation summary

Table 6 summarizes the notation.

AI Disclosure

An AI-assisted language model (Claude.ai, Anthropic) was used during manuscript preparation to assist in checking and verifying portions of the authors' own mathematical derivations and to improve clarity of presentation. The AI tool did not generate original results, proofs, or derivations. All mathematics, analyses, and conclusions were independently derived, reviewed, and validated by the authors, who take full responsibility for the content of the manuscript.

References

- [1] Redner S 2001 *A Guide to First-Passage Processes* (Cambridge: Cambridge University Press)
- [2] Rudnick J and Gaspari G 2004 *Elements of the Random Walk* (Cambridge: Cambridge University Press)
- [3] Spitzer F 1964 *Principles of Random Walk* (New York: Springer)
- [4] Feller W 1971 *An Introduction to Probability Theory and Its Applications* vol 2, 2nd edn (New York: Wiley)
- [5] Andersen E S 1962 The equivalence principle in the theory of fluctuations of sums of random variables *Colloquium on Combinatorial Methods in Probability Theory, Aarhus* pp 13–16
- [6] Zeller C and Cordery R 2020 Light scattering as a Poisson process and first-passage probability *J. Stat. Mech.* **2020** 063404
- [7] Kubelka P and Munk F 1931 *Z. Tech. Phys.* **12** 593–601
- [8] Chandrasekhar S 1960 *Radiative Transfer* (New York: Dover)
- [9] Sandoval C and Kim A D 2014 Deriving Kubelka–Munk theory from radiative transport *J. Opt. Soc. Am. A* **31** 628–636
- [10] Sandoval C and Kim A D 2017 Generalized Kubelka–Munk approximation for multiple scattering of polarized light *J. Opt. Soc. Am. A* **34** 153–162
- [11] Myrick M L, Simcock M N, Baranowski M, Brooke H, Morgan S L and McCutcheon J N 2011 The Kubelka–Munk diffuse reflectance formula revisited *Appl. Spectrosc. Rev.* **46** 140–165
- [12] Henyey L G and Greenstein J L 1941 Diffuse radiation in the galaxy *Astrophys. J.* **93** 70–83
- [13] Pfeiffer N and Chapman G H 2008 Successive order, multiple scattering of two-term Henyey–Greenstein phase functions *Opt. Express* **16** 13637–13645
- [14] Oste R and Van der Jeugt J 2015 Motzkin paths, Motzkin polynomials and recurrence relations *Electron. J. Combin.* **22**(2) P2.8

Table 6: Principal notation.

Symbol	Definition	Notes
<i>Scattering parameters</i>		
g	$\langle \cos \theta \rangle$	Anisotropy factor, $g \in [0, 1)$
μ	$\cos \theta$	Direction cosine
$P_{\text{HG}}(\mu; g)$	equation (4.1)	Henyey–Greenstein phase function
S	scattering coefficient	Units: inverse length
χ	absorption coefficient	Units: inverse length
<i>Random walk quantities</i>		
n	scattering order	Number of scattering events
m_s	path length	$\equiv n$; standard MC terminology, used in figures
n_p	peak count	Direction reversals
n_f	forward-flat count	Forward-preserving flat steps
c	step length	Distance between successive scattering events
<i>Step probabilities</i>		
r_b	backscattering probability	$3D \rightarrow 1D$ mapped parameter
r_f	forward-flat probability	Forward-preserving step
r	backward-step probability	1D model parameter
<i>BTF parameters</i>		
BTF	Boundary Truncation Factor	Equation (1.3)
$A(g)$	amplitude	$1 - g(1 + g)/2$
$m_x(g)$	width parameter	$4g/(1 - g)$
n_0	peak location	$= 2$ (minimum scattering order for return)
$\alpha(g)$	shape parameter	$1 + 0.033(g - 2/3)/(1 - g)$; equation (6.3)
<i>Algorithm quantities</i>		
$\mu_b(g)$	angular threshold	Separates effective forward/backward; equation (5.1)
$\gamma(g, n)$	effective exponent	$2 + \text{BTF}(n, g)(n - 2)$; equation (5.2)
$F(\mu; g)$	HG cumulative distribution	$\int_{-1}^{\mu} P_{\text{HG}}(\mu'; g) d\mu'$
$p_{r2}(g)$	two-step return probability	Exact result for $n = 2$
<i>Combinatorial objects</i>		
C_n	Catalan number	$(2n)!/(n!(n + 1)!)$
$M_n(t)$	Motzkin polynomial	Equation (2.4)
$T(n, k)$	Motzkin triangle coefficient	$n!/((n - 2k)! k! (k + 1)!)$

- [15] Drake D and Gantner R 2011 Generating functions for plateaus in Motzkin paths *Preprint* arXiv:1109.3272
- [16] Simon K and Trachsler B 2003 A random walk approach for light scattering in material *Discrete Math. Theor. Comput. Sci.* pp 289–300
- [17] OEIS Foundation Inc. 2024 The On-Line Encyclopedia of Integer Sequences <https://oeis.org> (sequences A000108, A026300)
- [18] Jacques S L 2010 Monte Carlo modeling of light transport in tissue (steady state and time of flight) *Optical-Thermal Response of Laser-Irradiated Tissue* 2nd edn (Berlin: Springer) pp 109–144
- [19] Sassaroli A, Blumetti C, Martelli F, Alianelli L, Contini D, Ismaelli A and Zaccanti G 1998 Monte Carlo procedure for investigating light propagation and imaging of highly scattering media *Appl. Opt.* **37** 7392–7400
- [20] Jacques S L 2013 Optical properties of biological tissues: a review *Phys. Med. Biol.* **58** R37–R61
- [21] Binzoni T, Leung T S, Gandjbakhche A H, Rüfenacht D and Delpy D T 2006 The use of the Henyey–Greenstein phase function in Monte Carlo simulations in biomedical optics *Phys. Med. Biol.* **51** N313–N322
- [22] Modrić D, Bolanča S and Beuc R 2009 Monte Carlo modeling of light scattering in paper *J. Imaging Sci. Technol.* **53** 020201
- [23] Carrillo R E, Aysal T C and Barner K E 2010 A generalized Cauchy distribution framework for problems requiring robust behavior *EURASIP J. Adv. Signal Process.* **2010** 312989 (pp 1–17)
- [24] Alzaatreh A, Lee C, Famoye F and Ghosh I 2016 The generalized Cauchy family of distributions with applications *J. Stat. Distrib. App.* **3** 12 (pp 1–16)